GeoScienceWorld
Lithosphere
Volume 2022, Article ID 5504977, 14 pages
https://doi.org/10.2113/2022/5504977

Lithosphere

*Research Article*

# Deep Electrical Structure of the Qilian Orogenic Belt with Dynamic Implications for the Northeastern Margin of the Tibetan Plateau: Revealed by 3D Magnetotelluric Inversion Using Unstructured Tetrahedral Elements

**Jianqiang Kang**,[1] **Jiangtao Han**,[1,2] **Rui Gao**,[3] **Zhonghua Xin**,[1] **Lijia Liu**,[1,2] **and Fanwen Meng**[1]

[1]*College of Geoexploration Science and Technology, Jilin University, Changchun, China*
[2]*Key Laboratory of Applied Geophysics, Changchun, China*
[3]*School of Earth Geosciences and Engineering, Sun Yat-sen University, Guangzhou, China*

Correspondence should be addressed to Jiangtao Han; hanjt@jlu.edu.cn

Received 12 April 2022; Revised 17 August 2022; Accepted 27 September 2022; Published 25 October 2022

Academic Editor: Shengsi Sun



We present the results of a magnetotelluric (MT) array across the Qilian orogenic belt to elucidate the uplift mechanism of the northeastern Tibetan Plateau (Qinghai-Tibet Plateau). The array extends from the Qaidam basin in the south to the southern edge of the Alxa block in the north. Using the three-dimensional (3D) inversion of MT data based on unstructured tetrahedral elements, the electrical structure 100 km below the orogenic belt is obtained. The results show that there are high-resistivity bodies in the lithospheric mantle of the North Qilian and Hexi Corridor, which may represent the trace of southward subduction of the Asian lithosphere. Besides, there are partially molten bodies with low resistivity in the middle and lower crust below the Qilian orogenic belt, which may be caused by tectonic heat. The melt fraction of low-resistivity bodies is 2-5%, which indicates that the crustal flow from the Qiangtang and Songpan-Ganzi blocks is unable to penetrate beneath the Qilian orogenic belt. The low-resistivity bodies beneath the Qilian orogenic belt decouples the upper crust from the middle-lower crust. Owing to the continuous compression, the decoupled middle-lower crust has subsequently driven the northward movement of the upper crust, resulting in the uplift of the Qilian orogenic belt.

## 1. Introduction

The northeastern margin of the Tibetan Plateau is distant from the Indian-Asian collision front. This margin consists primarily of the Qaidam, the Qilian orogenic belt, and Alxa block (a part of the North China Craton) from south to north. The area extending from the south of Tianshan to the north of Kunlun Mountain (e.g., the Tarim and Qaidam basins, Qilian Shan, and Alxa block) constituted a plate known as "the western plate" in the Late Proterozoic [1, 2]. NE-SW extension led to the opening of the North Qilian Ocean during the Neoproterozoic to Mid-Late Cambrian. The North Qilian Ocean underwent northward subduction and closed along the North Qilian suture during the Late Ordovician. The collision of the Qilian-Qaidam and Alxa blocks occurred due to the compressive stress regime associated with the closure of the North Qilian Ocean, and the North Qilian subsequently entered an orogenic stage. The surface expression of the Qilian orogenic belt was strongly denuded after the Late Devonian owing to continuous extension following collisional orogenesis. The Paleozoic orogeny in the Qilian area ceased completely in the Carboniferous. The Indian and Asian plates began to collide during the Cenozoic, with the strong compression of the Indian plate activating extensive orogenesis [3, 4].

The Tibetan Plateau has undergone an enormous amount of uplift since the Cenozoic [5, 6]. The outward growth and expansion of the plateau have been modeled

using several tectonic mechanisms, such as continuous shortening [7–9], crustal channel flow [10, 11], and rigid plate compression [5]. The Qilian orogenic belt, which is located in the front-most zone of outward expansion of the Tibetan Plateau, can be divided into three parts: the complex North Qilian, a transitional Middle Qilian, and the relatively simple, high-resistivity South Qilian [12–14]. Several irregularly shaped, unconnected "fragments" of extremely high-resistivity blocks in the mid-upper crust and a stratified low-resistivity layer in the mid-lower crust comprise the electrical structure of the crust in this area [15, 16]. Gao and Cheng [17] defined Kuantan Shan-Hei Shan fault (KHF) as the northern boundary thrust (NBT), which is similar to the thrust structure of the main Himalayan thrust (MHT) belt along the southern margin of the Tibetan Plateau, indicating northward thrusting of the Tibetan Plateau along this boundary. Furthermore, the subduction position of the Asian plate relative to the northeastern margin Tibetan Plateau is still disputed, particularly in the northern margin of the Qaidam basin and the lower part of the Qilian orogenic belt [18–20].

The MT inversion results of Liang et al. through the Qilian orogenic belt have found large-scale high-resistivity bodies dipping south under the Alxa block and isolated conductive bodies in the middle-lower crust of the orogenic belt [21]. Since the degree of freedom of 3D inversion of single profile is significantly increased, there is a risk of introducing false anomalies [22]. To reduce this risk and further study the mechanism governing the outward expansion and growth of the Tibetan Plateau, we added 35 additional stations to build a 3D dataset (red dots in Figure 1(b)), providing more constraints for the model. In addition, we used unstructured tetrahedral elements for 3D inversion, which can fit more complex geological structures [23].

## 2. Data and Methods

*2.1. Data Collection and Processing.* The MT array mainly transected the Qilian orogenic belt, extending from the northern margin of the Qaidam basin to the southern margin of the Alxa block and passing through Muli, Tianjun, and Gaotai cities. A total of 128 MT stations (blue and red dots in Figure 1(b)) were recorded to form an approximate 3D array, of which the new stations were recorded in 2019. The total length of profile L1 is 550 km (white solid line in Figure 1(b)), with 93 stations, and the average station spacing was 5 km. The electrical structure of this profile has been published by Liang et al. [21]. The MT data were collected using the Phoenix V5-2000 system (Phoenix Geophysics, Canada), with an average recording time of >20 h. The three mutually orthogonal magnetic field components (Hx, Hy, and Hz) and two mutually orthogonal horizontal electric field components (Ex and Ey) were recorded for each station. The $x$, $y$, and $z$ subscripts indicate the north-south, east-west, and vertical directions, respectively. The original MT time series data were transformed into the frequency domain after data collection, with the frequency-dependent transfer function computed using a statistically robust algorithm [26]. Finally, the MT data up to 2000 s was obtained.

Figure 2 shows the apparent resistivity and phase curves for typical measuring stations that sample the different geological units along the transect (yellow triangles in Figure 1(b)). It can be seen that the sounding data are generally with relatively high quality.

*2.2. Dimensionality Analysis.* The MT data dimensionality should be ascertained prior to the MT inversion. We used phase tensors to assess the dimensionality of the resistivity structures. A phase tensor can be drawn as an ellipse defined by the minimum phase ($\varphi$ min), maximum phase ($\varphi$ max), azimuth of the reference axis ($\alpha$), and skew angle ($\beta$). When the $\beta$ is greater than 3°, it indicates that the underground structure is three-dimensional features [27]. Figure 3 shows the phase tensor ellipses and corresponding absolute skew angles ($\beta$) at the MT stations for four observational periods (0.1, 1, 100, and 1000 s). The 0.1 and 1 s periods generally possess smaller absolute $\beta$ values (<3°), which imply that the shallow regional electrical structure primarily consists of 2D features. Larger absolute $\beta$ values (>3°) are observed at the 100 and 1000 s periods for some of the MT stations in the Qaidam basin and Qilian orogenic belt, which are indicative of 3D features (Figure 3). We therefore conclude that a 3D inversion approach is applicable for our MT data.

*2.3. Inversion*

*2.3.1. Data Inversion.* The MT data were inverted using the new 3D inversion program-GEM3D [23, 28]. In this new inversion code, the model is discretized by unstructured grids to better fit the complex underground structures. In addition, this program uses the limited-memory quasi-Newton (L-BFGS) inversion algorithm, which avoids the calculation of Hessian matrices and sensitivity matrices, greatly reduces the memory requirements, and improves the efficiency of 3D inversion [23, 29].

The full impedance tensors ($Z$) of 128 MT stations in the frequency range of 10–0.0005 Hz with 20 frequencies in total constituted the input data. For the off-diagonal elements, the error floor was set at 5% of $|\mathrm{Zxy} \times \mathrm{Zyx}|^{1/2}$. Since the diagonal elements were more susceptible to noise [30], we set the error floor at 20% of $|\mathrm{Zxy} \times \mathrm{Zyx}|^{1/2}$ for the diagonal elements. Unstructured tetrahedral elements were used for mesh generation (Figure 4). The overall grid size was 8000 km × 8000 km × 4000 km in $X \times Y \times Z$ direction. It contains 2000 km of air layer in $Z$ direction. The total number of elements was 1203521. The mesh in the central portion of the domain, which includes MT stations, was finer. We called it the core region. The grid size of this region was 500 km × 400 km × 100 km in $X \times Y \times Z$ direction. The area near the MT stations was meshed with a tetrahedral element size of 5-20 m. The part of the core region not near the MT stations was meshed with a tetrahedral element size of 0.1-10 km. The final three-dimensional mesh was generated using the TetGen mesh generator [31]. The initial model was set to a uniform half space of 100 Ω·m. And the initial $\lambda$ was set to 100. When the relative change in overall root mean square (RMS) between two consecutive iterations was below 2%, it was then divided by 10. After 110

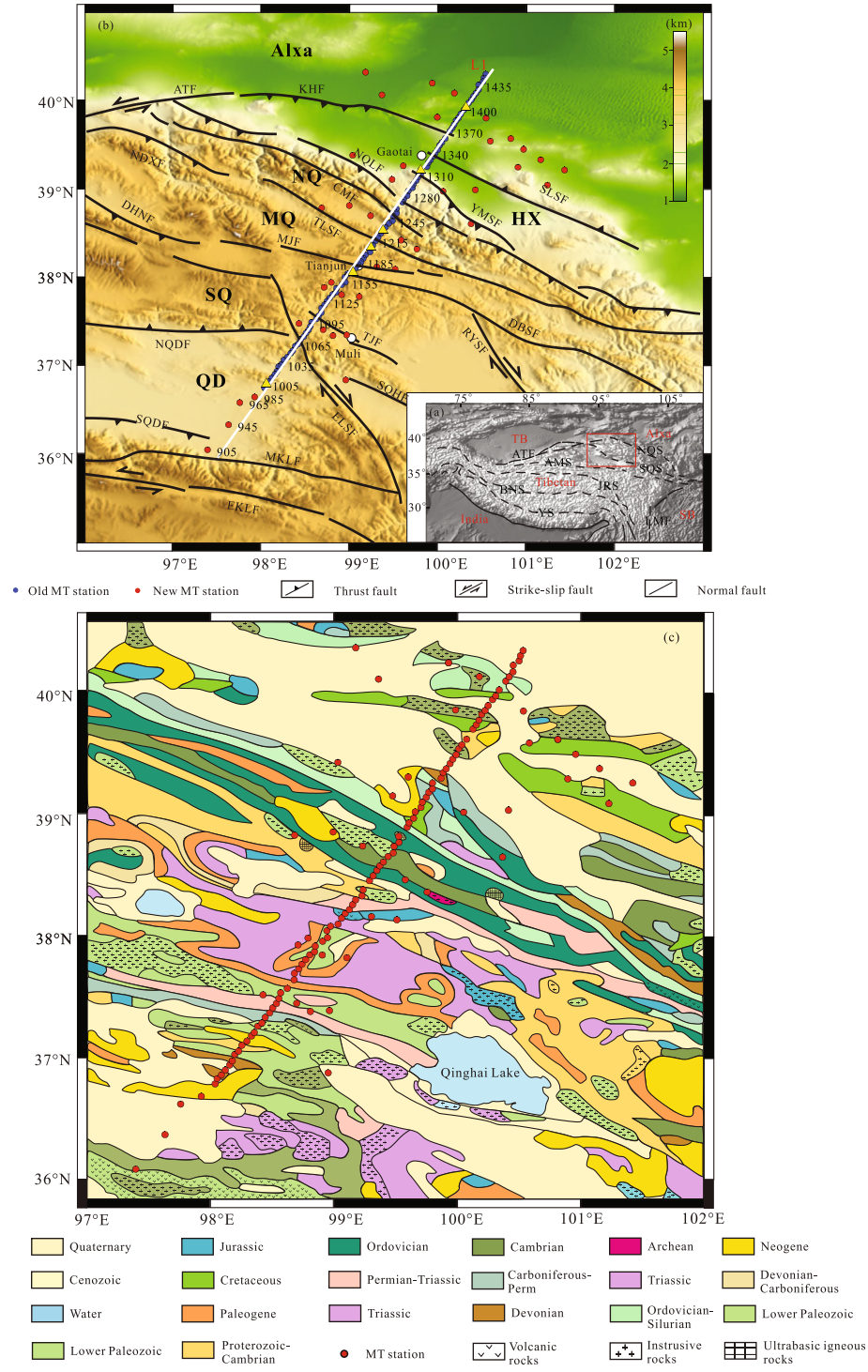


FIGURE 1: (a) Topography and major tectonic structures of the Tibetan Plateau and the surrounding region. The red rectangle outlines the present study area. YS: Yalu suture; BNS: Bangong-Nujiang suture; JRS: Jinsha River suture; AMS: Animaqing suture; SQS: South Qilian suture; NQS: North Qilian suture; ATF: Altyn Tagh fault; LMF: Longmenshan fault; TB: Tarim basin; SB: Sichuan basin. (b) Details of the MT station locations and the major tectonic structures in the present survey area (after Deng et al. [24]). The yellow triangles are the locations of the stations selected for showing resistivity and phase curves in Figure 2. The white solid line is the profile L1 used for Figure 6. QD: Qaidam; SQ: South Qilian; MQ: Middle Qilian; NQ: North Qilian; HX: Hexi Corridor; KHF: Kuantan Shan-Hei Shan fault; ATF: Altyn Tagh fault; YMSF: Yumu Shan fault; SLSF: Southern Longshou Shan fault; NQLF: Northern Qilian fault; CMF: Changma fault; NDXF: Northern Daxue Shan fault; TLSF: Tuolai Shan fault; MJF: Muli-Jiangchang fault; DHNF: Danghenan Shan fault; TJF: Tianjun fault; DBSF: Daban Shan fault; ELSF: Elashan fault; NQDF: Northern Qaidam fault; SQHF: Southern Qinghainan Shan fault; RYSF: Riyue Shan fault; SQDF: Southern Qaidam fault; EKLF: Eastern Kunlun fault; MKLF: Middle Kunlun fault. (c) Simplified geologic map of the study area (modified from Steinshouer et al. [25]).

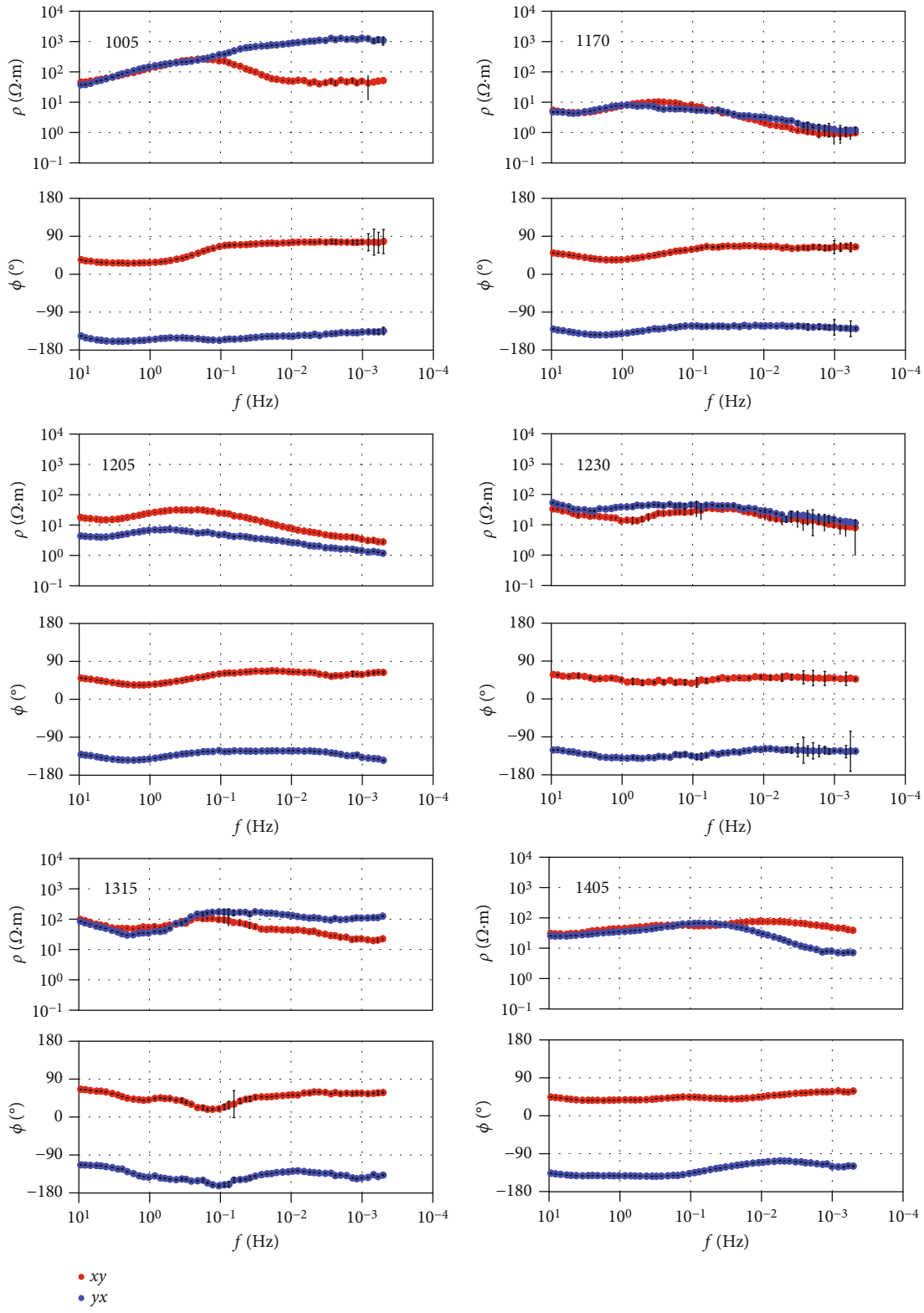


Figure 2: Typical apparent resistivity and phase curves. Red dots: XY component; blue dots: YX component. Station 1005 is located in the Qaidam basin. Station 1170 is located in the South Qilian. Stations 1205 and 1230 are located in the Middle and North Qilian. Station 1315 is located in the Hexi Corridor. Station 1405 is located in the Alxa block.

iterations, the RMS reduced from 18.11 to 2.97. Figure 5 shows the distribution of RMS. The RMS of most stations is less than 3, indicating that our inversion model is well constrained by the observed data. The apparent resistivity phase fitting curve of each station on profile L1 is shown in Figure S1 of the Supplementary Materials. The Niblett-

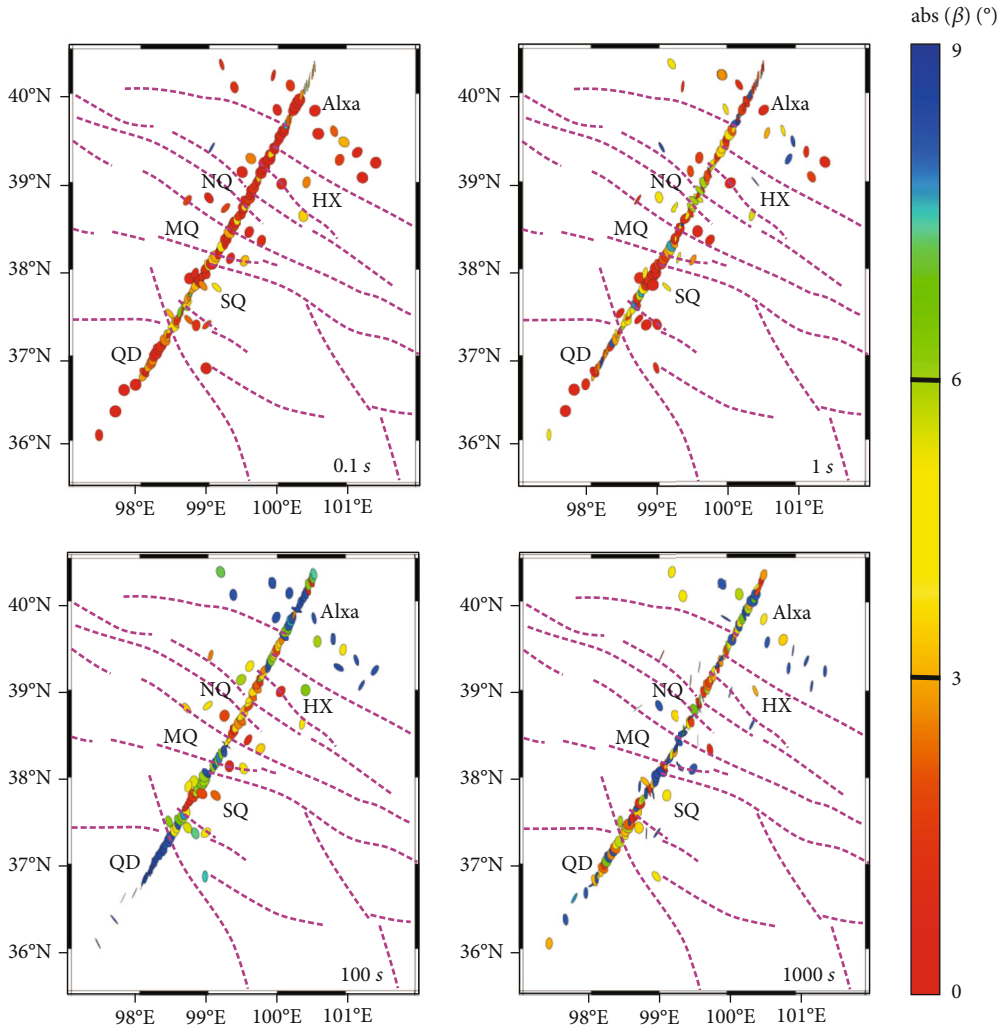


FIGURE 3: Phase tensor ellipses and corresponding absolute skew angles ($\beta$) at the MT sites for the 0.1, 1, 100, 1000 s periods. The colors represent the absolute $\beta$ values. QD: Qaidam; SQ: South Qilian; MQ: Middle Qilian; NQ: North Qilian; HX: Hexi Corridor.

Bostick method [32] was used to estimate the penetration depth of each station in L1 profile (Figure S2 in Supplementary Materials).

*2.3.2. Inversion Results.* The electrical structural model of profile L1 obtained by the inversion is shown in Figure 6; the red areas (C1–C3) represent relatively low-resistivity areas, and the blue areas (R1–R3) represent relatively high-resistivity areas. We also marked the Moho depth in this region based on the deep geophysical results from a previous study [33]. Figure 7 shows 4 map view slices at depths of 5, 20, 40, and 60 km, respectively. Because there are additional stations in the Qaidam basin, compared with the previous electrical structure of Liang et al. [21], our results show that the high-resistivity body R1 in the Qaidam basin is larger in scale and may extend below the Moho. In addition, in the northeast of the study area, we have arranged new stations along both sides of the profile L1, which provides more constraints for the model. The new inversion result shows that there is a medium- to high-resistivity body R3 under the Moho of North Qilian and Hexi Corridor, and the shallow part is connected with the high-resistivity body R2 under the Alxa block (Figure 6(b)). The inversion results at 5 km depth show that the shallow part of the Qilian orogenic belt is characterized by high resistivity (Figure 7(a)), which may be related to the surface exposed Ordovician-Silurian rock bodies and arc associations, ophiolitic melanges, and low- to high-grade metamorphic rocks [34]. The most obvious characteristic of the electrical structure is that the middle-lower crust of the Qilian orogenic belt possesses low-resistivity bodies C1, C2, and C3. The Alxa block is a relatively stable block with a high-resistivity crust.

Sensitivity tests were conducted to verify the reliability of the final inversion model. In order to verify whether the high conductivity anomalies C1 and C2 in the inversion model were reliable, we replaced the resistivity value in the rectangular area at the depths 20-50 km with 100 Ω·m (Figure 8(a)). The modified model raised the RMS value from 2.97 to 3.24. For difference quantification in the RMS

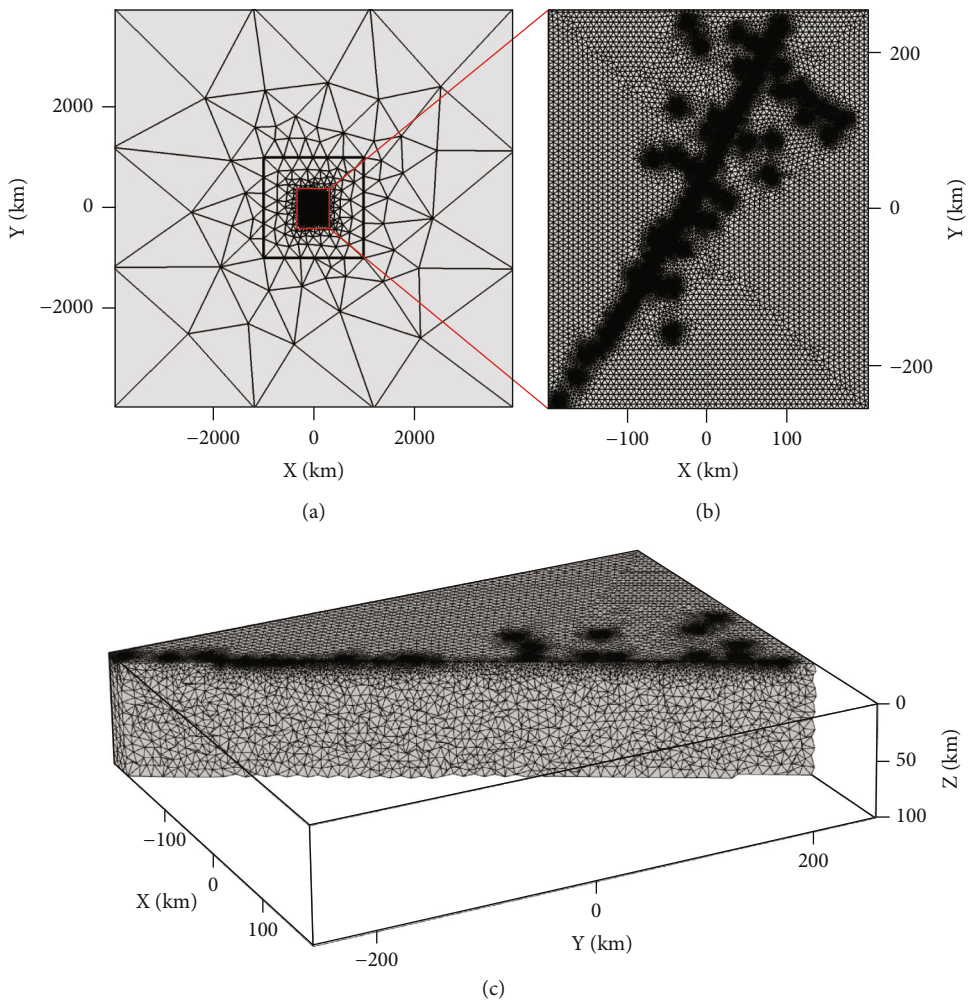


FIGURE 4: Computational mesh used in the 3D inversion. (a) Overall view; (b) mesh around the survey area; (c) subsurface area without air elements along profile L1.

misfits between different models, we utilized the RMS_Update parameter [35, 36], defined as

$$\text{RMS\_Update} = \frac{|\text{RMS}_1\text{-RMS}_0|}{\text{RMS}_0}, \quad (1)$$

where $\text{RMS}_0$ is the misfit value of the selected inversion model and $\text{RMS}_1$ is the misfit value of the test model. Site-by-site RMS_Update values are plotted in Figure 8(b), which shows a systematic change in RMS_Update at the stations above C1-C2 in the test model. We conducted the same test on high conductivity anomalies C3 (Figure S3 in Supplementary Materials).

In addition, we also conducted a sensitivity test on the high-resistivity anomaly R3, by replacing the resistivity value in the rectangular area at the depths 60-100 km with 10 Ω·m (Figure 9(a)). The RMS of the modified model was 3.19, and the RMS_Update of the stations above R3 has changed significantly (Figure 9(b)).

## 3. Discussion

*3.1. Location of Asian Lithospheric Subduction Relative to the Tibetan Plateau.* The subduction position of the Asian plate relative to the Tibetan Plateau is still disputed. In our result, we observe that high-resistivity body R3 is located primarily under the North Qilian and Hexi Corridor (Figure 6(b)). The deeper section of R3 wedges southward into the lower part of the mantle of the North Qilian, forming a high angle. The shallow section is associated with high-resistivity basement R2 of the Alxa block, which has manifested into a wedging feature that begins at the hard North China Plate and extends to the lower part of the relatively weak North Qilian orogenic belt. The electrical structure of adjacent MT profiles also found high-resistivity bodies wedged southward under the Hexi Corridor and Alxa block [13, 16]. The results of seismic tomography show that there is high-velocity anomalies inserted southward by the Alxa block under the Qilian orogenic belt [20, 37]. The anisotropy of the orogenic belt reflects that it is affected by the southward subduction of the

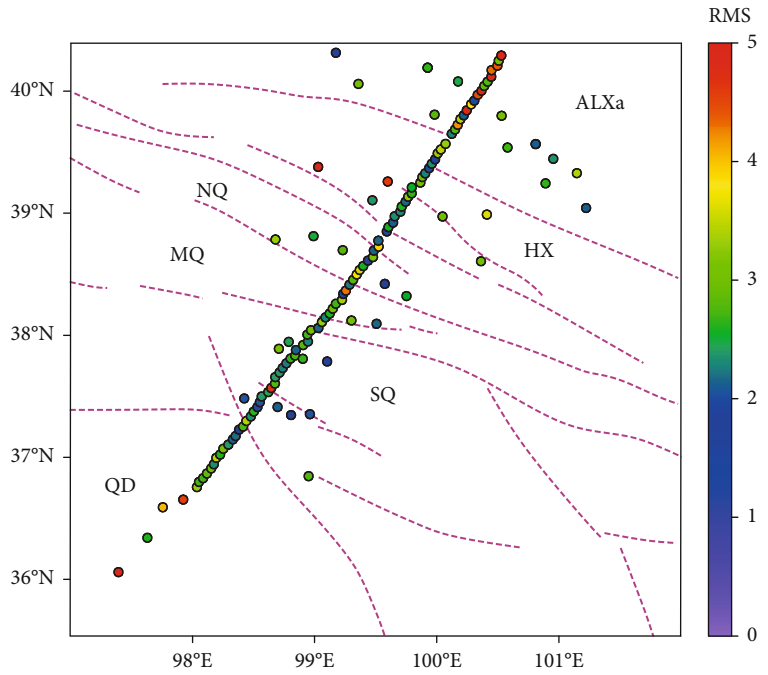


Figure 5: Values of RMS at MT stations. QD: Qaidam; SQ: South Qilian; MQ: Middle Qilian; NQ: North Qilian; HX: Hexi Corridor.

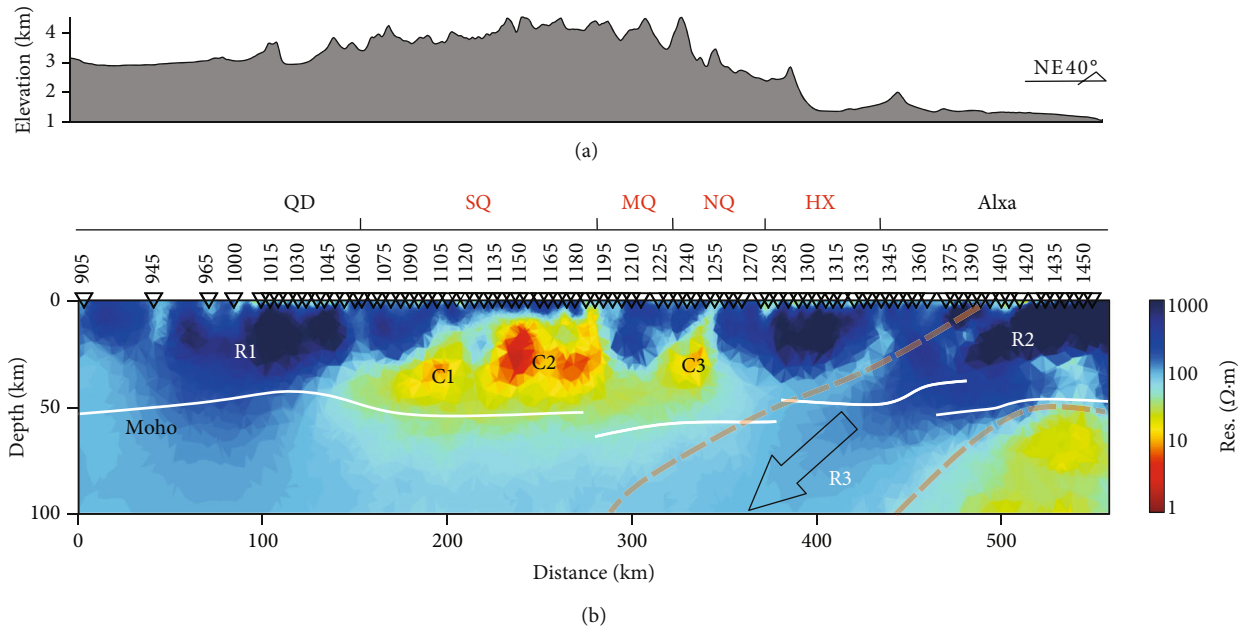


Figure 6: Inversion result of profile L1. (a) Topography along the profile L1. (b) Three-dimensional MT inversion results of profile L1 and interpretation. Inverted triangles at the top denote MT station locations. QD: Qaidam; SQ: South Qilian; MQ: Middle Qilian; NQ: North Qilian; HX: Hexi Corridor.

lithosphere of the northern block [38]. Besides, the results of receiver function show that there is a south-dipping LAB under the Alxa block and the North Qilian [19]. A south-dipping reflection interface has been identified in a deep seismic reflection profile along the North Qilian-Hexi Corridor [39]. The reactivation of the Haiyuan fault during the Late Miocene may be affected by the southward subduction of the North China Plate [19, 40, 41]. All these results indicate that the contribution of the North China Plate to the northeastern lateral growth of the Tibetan Plateau is not due to passive blockage but rather active wedging to the side of the Tibetan Plateau. R3 may represent subducted Asian lithosphere. The results of Liang et al. also found traces of southward subduction of the Alxa

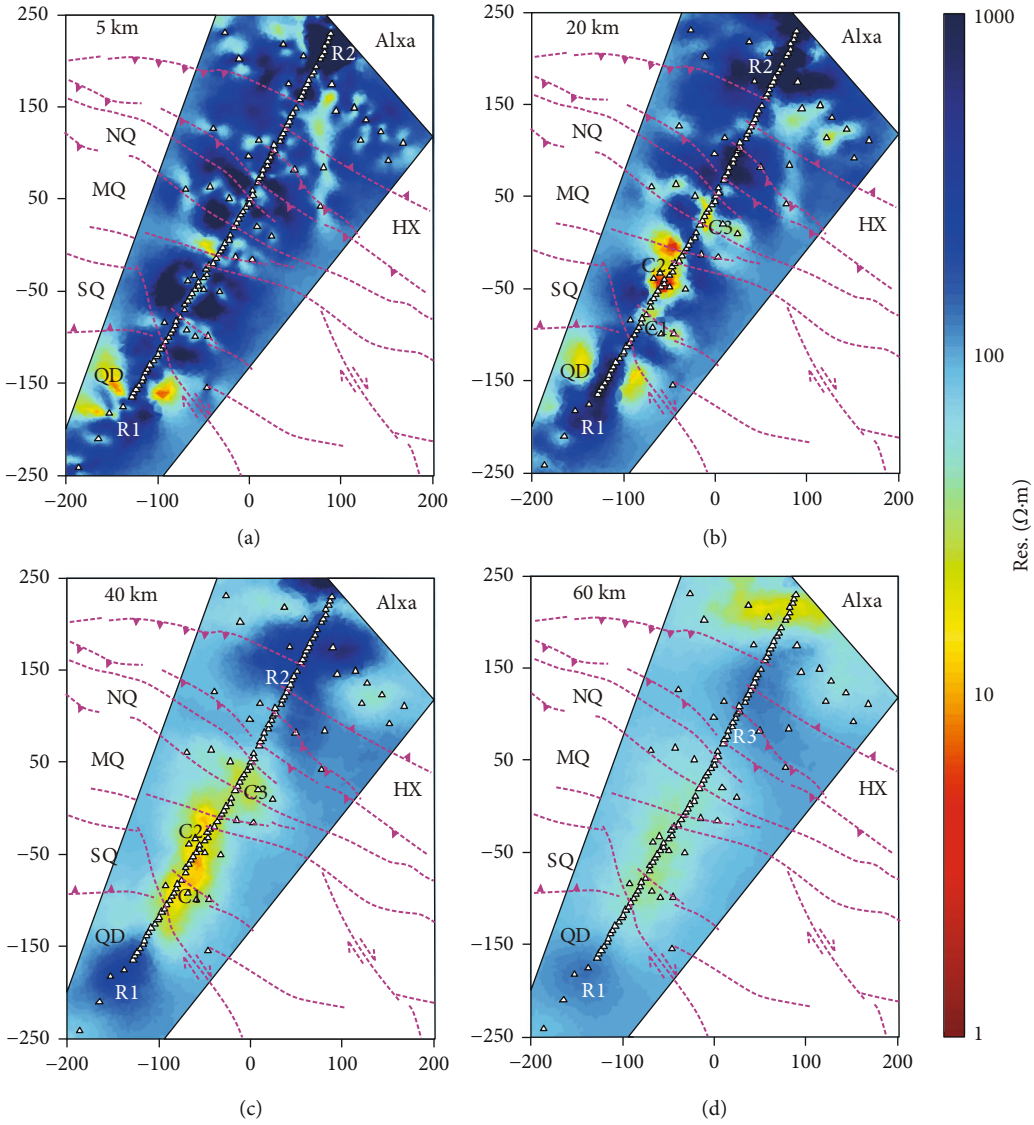


FIGURE 7: Horizontal slices of three-dimensional electrical model at different depths. QD: Qaidam; SQ: South Qilian; MQ: Middle Qilian; NQ: North Qilian; HX: Hexi Corridor.

block [21]. On this basis, we believe that the Asian lithospheric mantle has been subducted under the North Qilian orogenic belt.

*3.2. Low Resistivity Bodies beneath Qilian Orogenic Belt.* The electrical structure of the Qilian orogenic belt is obviously different to that of the Qaidam basin. Low-resistivity bodies C1–C3 are present in the middle and lower crust. Horizontal slices at different depths also show that there are low-resistivity bodies in the depth range of 20-60 km below the Qilian orogenic belt (Figure 7). Recent seismic studies have indicated that there is a low-velocity zone that corresponds to the low-resistivity zone in the middle and lower crust of the Middle and North Qilian [19, 42]. The genesis of low resistivities is usually related to graphite, sulfide minerals, partial melting, and fluids [43, 44]. Graphite films do not remain intact at high temperatures [45]. The temperature of the lower crust below the North Qilian can reach 600–840°C [46], which would result in unstable graphite films. The distribution range of low-resistivity anomalies that are produced by sulfide minerals is limited [43], whereas low-resistivity bodies C1–C3 cover a large area in our imaged electrical structure. Multiple lines of evidence have indicated that the low resistivities in the middle and lower crust of the Tibetan Plateau are closely related to partial melting and/or aqueous fluids [10, 47, 48]. In the front of the subduction of the Indian plate, there are also low-resistivity bodies in the middle and lower crust of the South Lhasa terrane, which may be a partial melting caused by tectonic heat [49]. The far-field effect of the convergence of Indo-Asian since the Cenozoic can affect the northeast of the Asian plate [50, 51]. Affected by the southward subduction of the Asian plate and the far-field effect of the northward advancement of the Indian plate, the Qilian orogenic belt is in a compressional setting and the crust undergoes napping deformation [5, 19, 21]. In addition, the middle-lower crust

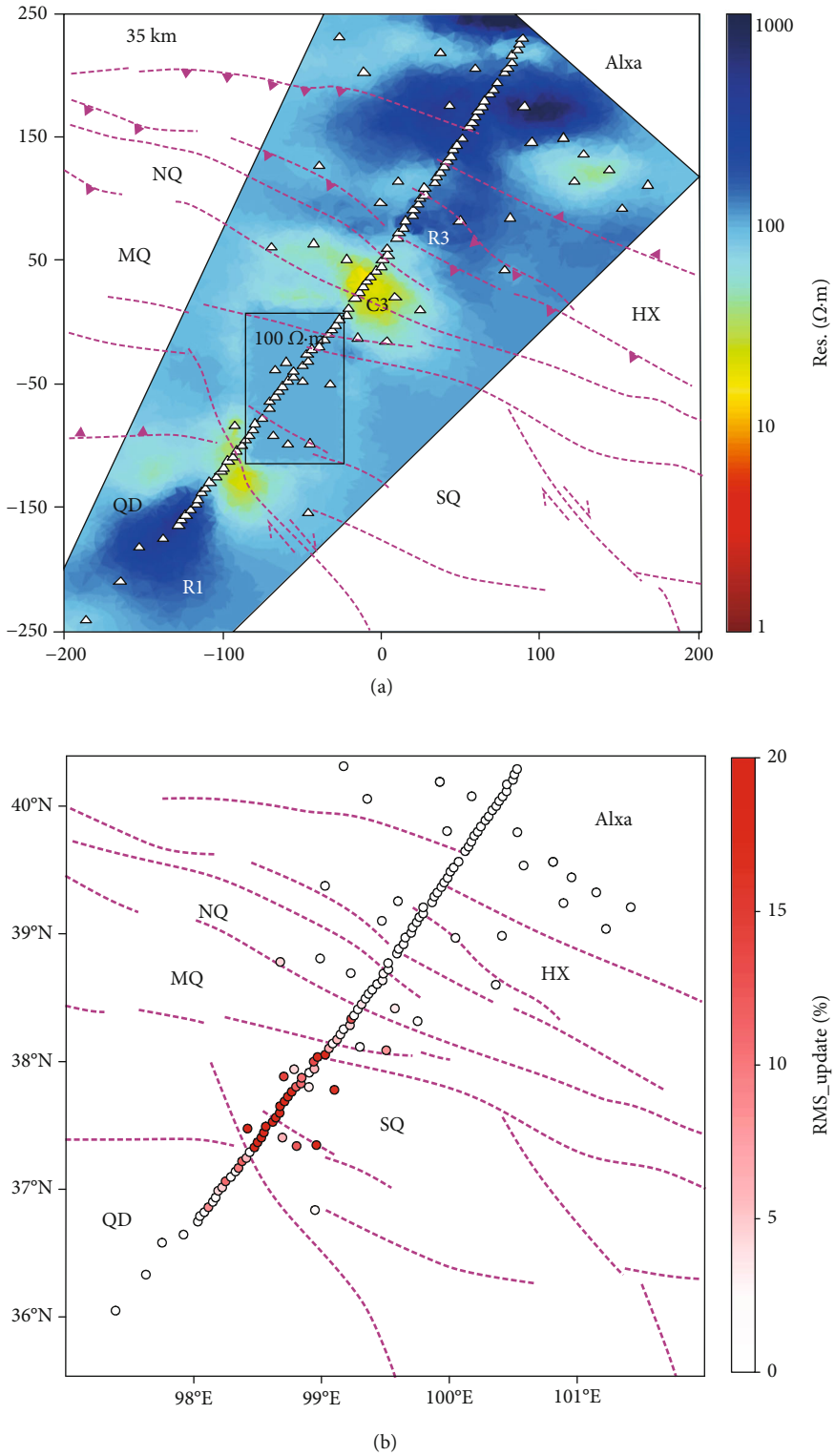


FIGURE 8: Sensitivity tests of C1 and C2. (a) The rectangle area surrounding C1-C2 is replaced with a homogeneous value of 100 Ω·m. (b) Values of RMS_Update for a 3-D forward modified model.

of the Qilian orogenic belt is rather felsic. Under the same temperature and pressure conditions, felsic rocks are generally weaker than intermediate/mafic rocks [52], which will weaken the middle-lower crust [53]. Zhao et al. believe that shear heating is the origin of low-velocity zone in the middle and lower crust of the Qilian orogenic belt [53]. Besides, the crustal nappe deformation generates frictional heating [49]. Therefore, the tectonic heat may be enough to partially melt the middle and lower crust, leading to lower resistivities.

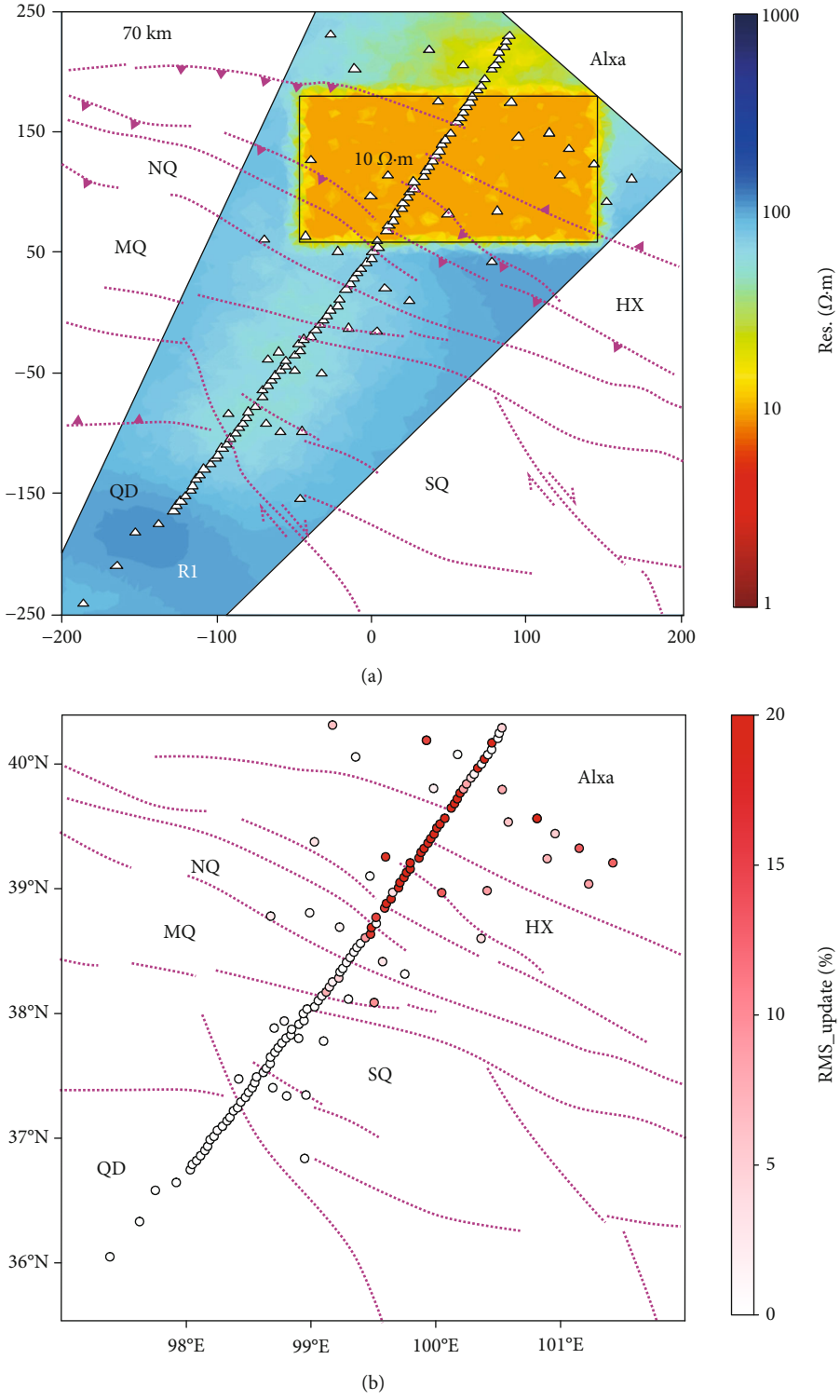


Figure 9: Sensitivity tests of R3. (a) The rectangle area surrounding R3 is replaced with a homogeneous value of 10 Ω·m. (b) Values of RMS_Update for a 3-D forward modified model.

*3.3. The Uplift Model of the Qilian Orogenic Belt.* The underlying causes of the Tibetan Plateau's uplift are somewhat controversial [5, 7, 11]. The potential existence of crustal flow in the northeastern Tibetan Plateau also remains a controversial topic [54]. Our inversion results indicate that the crust of the Qaidam basin shows a high-resistivity R1. The Qaidam basin was a part of the Precambrian craton, which was called the Qilian-Qaidam Craton [3]. R1 may represent the rigid crust of the craton. Due to the blocking effect of the rigid crust in the

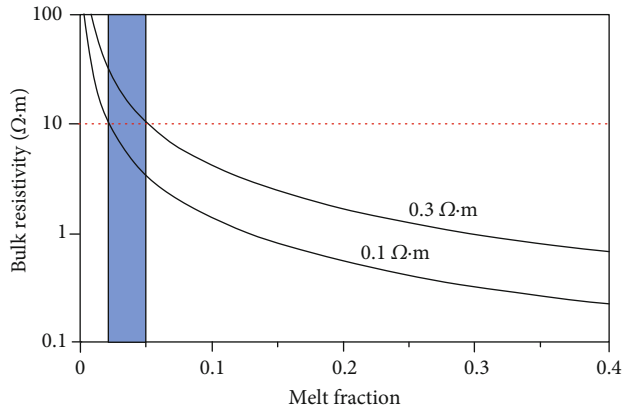


FIGURE 10: When the resistivity of pure melt is 0.1 and 0.3 Ω·m, respectively, the relationship between melt fraction and bulk resistivity is calculated by Archie's formula. The bulk resistivity of C2 is about 10 Ω·m.

Qaidam basin, crustal flow does not penetrate beneath the Qilian orogenic belt. Our results show that there are only local and small-scale high conductors under the Qilian orogenic belt, which is significantly different from the large-scale interconnected high conductors under the Qiangtang and Songpan-Ganzi blocks, where crustal flow is widely developed [10, 47, 48].

Archie's formula can be used to calculate the melt fraction of conductors, which can be expressed as

$$\rho_f = C^{-1}\phi_m^{-n}\rho_m, \tag{2}$$

where $C$ and $n$ are empirical coefficients and are 1.47 and 1.3 for low melt fractions, respectively [55]; $\varphi_m$ is the melt fraction; $\rho_m$ is the resistivity of pure melt (usually 0.1–0.3 Ω·m) [44, 56]; and $\rho_f$ is the bulk resistivity. For the largest high conductor C2 under the Qilian orogenic belt, $\rho_f$ is 10 Ω·m.

According to the Archie's formula, the melt fraction of C2 is estimated in Figure 10, which is in the range of 2–5%, and is far less than the melt fractions of high conductors below the Qiangtang and Songpan-Ganzi blocks [57]. Besides, laboratory studies have shown that crustal flow is possible only when the melt fraction is greater than 5%, because in this case, the strength and viscosity of rock will be reduced by an order of magnitude [44, 55, 58]. It therefore seems highly unlikely that channel flow is responsible for the enhanced thickness of the lower crust.

Earlier studies have revealed the existence of a low-velocity layer in the Qilian orogenic belt [19, 42] that may be a weak layer in the crust [59]. Recent studies have also revealed that seismic anisotropy exists in both the mid-upper crust and upper mantle of this region [60, 61], such that the presence of low-resistivity bodies may indicate that the deformation in the upper and middle-lower crust is decoupled in this region. The lithospheric mantle of the North China Craton was continuously squeezed into the lower part of the Qilian orogenic belt owing to continuous compression between the North China Craton and the northeastern margin of the Tibetan Plateau. This caused the decoupled middle-lower crust driving the upper crust northward, as well as strong deformation in the upper crust and an outward thrust, which resulted in the uplift of the Qilian orogenic belt and generated a series of thrust fault [34, 62, 63].

## 4. Conclusions

We acquired an MT array across the Qilian orogenic belt in the northeastern margin of the Tibetan Plateau, and the unstructured tetrahedral element is used for 3D inversion of MT data to constrain the deep electrical structure of the region. Similar to the previous result of Liang et al., we found traces of southward subduction of the Asian plate, but the new electrical structure shows that there are medium- to high-resistivity bodies below the Moho of the North Qilian and Hexi Corridor, which indicates that the Asian lithospheric mantle has been subducted southward beneath the North Qilian orogenic belt. We also found that there are low-resistivity bodies beneath the Qilian orogenic belt, but this may be partial melting caused by tectonic heat. The melt fraction of the low-resistivity body calculated by Archie's formula is 2-5%. Finally, we believe that there is no crustal flow beneath the Qilian orogenic belt. The lithospheric mantle of the North China Craton has been continuously squeezed into the lower part of the Qilian orogenic belt owing to continuous compression and convergence between the northeastern margin of the Tibetan Plateau and the North China Craton. The decoupled middle-lower crust has subsequently driven the northward movement of the upper crust, such that the Paleozoic sedimentary strata in the Qilian orogenic belt have undergone strong deformation and outward thrusting, resulting in its uplift.

## Data Availability

MT data used to support the 3D electrical structure is included in this article. Please ask for permission for further use of the data.

## Conflicts of Interest

The authors declare there are no competing interests.

## Acknowledgments

This study was sponsored by the National Natural Science Foundation of China (Grants 41590863, 41430213, and 41504076), National Key R&D Program of China (Grant 2017YFC0601305), Central University Basic Scientific Research Business Expenses Special Funds, and Jilin Province Science and Technology Development Plan Project (Grant 20180101093JC). Some figures were created using the GMT software package [64].

## Supplementary Materials

The supplementary materials include the apparent resistivity phase curves of all stations of profile L1, the estimated penetration depth of each station of L1, and the sensitivity test of C3. *(Supplementary Materials)*

## References


[1] Y. M. Feng and H. Q. Wu, "Tectonic evolution of north Qilian mountains and its neighbourhood since paleozoic," *Northwest Geoscience*, vol. 2, pp. 61–74, 1992.

[2] X. H. Ge and J. L. Liu, "Formation and tectonic background of the northern Qilian orogenic belt," *Earth Science Frontiers*, vol. 6, pp. 223–230, 1999.

[3] S. Song, Y. Niu, L. Su, and X. Xia, "Tectonics of the north Qilian orogen, nw China," *Gondwana Research*, vol. 23, no. 4, pp. 1378–1401, 2013.

[4] S. Song, L. Zhang, Y. Niu, L. Su, B. Song, and D. Liu, "Evolution from oceanic subduction to continental collision: a case study from the Northern Tibetan Plateau based on geochemical and geochronological data," *Journal of Petrology*, vol. 47, no. 3, pp. 435–455, 2006.

[5] P. Tapponnier, Z. Xu, F. Roger et al., "Oblique stepwise rise and growth of the Tibet Plateau," *Science*, vol. 294, no. 5547, pp. 1671–1677, 2001.

[6] A. Yin and T. M. Harrison, "Geologic evolution of the Himalayan-Tibetan orogen," *Annual Review of Earth and Planetary Sciences*, vol. 28, no. 1, pp. 211–280, 2000.

[7] P. England and G. Houseman, "Finite strain calculations of continental deformation: 2. Comparison with the India-Asia collision zone," *Journal of Geophysical Research: Solid Earth*, vol. 91, no. B3, pp. 3664–3676, 1986.

[8] X. Huang, R. Gao, X. Guo, W. Li, and X. Xiong, "Deep crustal structure beneath the junction of the Qilian Shan and Jiuxi basin in the northeastern margin of the Tibetan Plateau and its tectonic implications," *Chinese Journal of Geophysics*, vol. 61, no. 9, pp. 3640–3650, 2018.

[9] P. Zhang, Z. Shen, M. Wang et al., "Continuous deformation of the Tibetan Plateau from global positioning system data," *Geology*, vol. 32, no. 9, pp. 809–812, 2004.

[10] D. Bai, M. Unsworth, M. Meju et al., "Crustal deformation of the eastern Tibetan Plateau revealed by magnetotelluric imaging," *Nature Geoscience*, vol. 3, no. 5, pp. 358–362, 2010.

[11] M. Clark and L. Royden, "Topographic ooze: building the eastern margin of Tibet by lower crustal flow," *Geology*, vol. 28, no. 8, pp. 703–706, 2000.

[12] W. Xiao, B. Windley, Y. Yong et al., "Early Paleozoic to Devonian multiple-accretionary model for the Qilian Shan, NW China," *Journal of Asian Earth Sciences*, vol. 35, no. 3-4, pp. 323–333, 2009.

[13] Q. Xiao, J. Zhang, J. Wang, G. Zhao, and J. Tang, "Electrical resistivity structures between the northern Qilian Mountains and Beishan block, NW China, and tectonic implications," *Physics of the Earth and Planetary Interiors*, vol. 200-201, pp. 92–104, 2012.

[14] Q. Xiao, G. Shao, G. Yu, J. Cai, and J. Wang, "Electrical resistivity structures of the Kunlun-Qaidam-Qilian system at the northern Tibet and their tectonic implications," *Physics of the Earth and Planetary Interiors*, vol. 255, pp. 1–17, 2016.

[15] S. Jin, L. Zhang, Y. Jin, W. Wei, and G. Ye, "Crustal electrical structure along the Hezuo-Dajing profile across the northeastern margin of the Tibetan Plateau," *Chinese Journal of Geophysics*, vol. 55, no. 12, pp. 3979–3990, 2012.

[16] S. Xia, X. Wang, G. Min et al., "Crust and uppermost mantle electrical structure beneath Qilianshan orogenic belt and Alxa block in northeastern margin of the Tibetan Plateau," *Chinese Journal of Geophysics*, vol. 62, no. 3, pp. 950–966, 2019.

[17] R. Gao and X. Cheng, "Lithospheric structure and geodynamic model," *Himalaya and Tibet: mountain roots to mountain tops*, vol. 328, p. 9, 1999.

[18] M. Feng, P. Kumar, J. Mechie et al., "Structure of the crust and mantle down to 700 km depth beneath the east Qaidam basin and Qilian Shan from P and S receiver functions," *Geophysical Journal International*, vol. 199, no. 3, pp. 1416–1429, 2014.

[19] Z. Ye, R. Gao, Q. Li et al., "Seismic evidence for the North China plate underthrusting beneath northeastern Tibet and its implications for plateau growth," *Earth and Planetary Science Letters*, vol. 426, pp. 109–117, 2015.

[20] D.-X. Yu, Y.-H. Li, Q.-J. Wu, J.-T. Pan, F.-X. Zhang, and J. He, "S-wave velocity structure of the northeastern Tibetan Plateau from joint inversion of Rayleigh wave phase and group velocities," *Chinese Journal of Geophysics*, vol. 57, no. 3, pp. 800–811, 2014.

[21] H. Liang, R. Gao, S. Xue, and J. Han, "Electrical structure of the middle Qilian Shan revealed by 3-D inversion of magnetotelluric data: new insights into the growth and deformation in the northeastern Tibetan Plateau," *Tectonophysics*, vol. 789, article 228523, 2020.

[22] W. Cumming and R. Mackie, "Resistivity imaging of geothermal resources using 1D, 2D and 3D MT inversion and TDEM static shift correction illustrated by a Glass Mountain case history," in *Proceedings World Geothermal Congress*, pp. 25–29, Bali, Indonasia, 2010.

[23] X. Cao, C. Yin, B. Zhang, X. Huang, Y. H. Liu, and J. Cai, "3D magnetotelluric inversions with unstructured finite-element and limited-memory quasi-Newton methods," *Applied Geophysics*, vol. 15, no. 3-4, pp. 556–565, 2018.

[24] Q. Deng, P. Zhang, Y. Ran, X. Yang, W. Min, and Q. Chu, "Basic characteristics of active tectonics of China," *Science in China Series D: Earth Sciences*, vol. 46, no. 4, pp. 356–372, 2003.

[25] D. Steinshouer, J. Qiang, P. McCabe, and R. Ryder, *Maps showing geology, oil and gas fields, and geologic provinces of the Asia Pacific region: U.S. Geological Survey*, Open-File Report 97-470-F, 1999.

[26] G. Egbert, "Robust multiple-station magnetotelluric data processing," *Geophysical Journal International*, vol. 130, no. 2, pp. 475–496, 1997.

[27] T. Caldwell, H. Bibby, and C. Brown, "The magnetotelluric phase tensor," *Geophysical Journal International*, vol. 158, no. 2, pp. 457–469, 2004.

[28] Y. Liu, J. Zhang, C. Yin et al., "GEM3D: a 3D inversion code for geophysical electromagnetic data based on unstructured tetrahedron grid," in *International Workshop on Gravity, Electrical & Magnetic Methods and Their Applications*, vol. 19-22, pp. 416–419, Xi'an, China, 2019.

[29] D. Avdeev and A. Avdeeva, "3D magnetotelluric inversion using a limited-memory quasi-Newton optimization," *Geophysics*, vol. 74, no. 3, pp. F45–F57, 2009.

[30] J. Gao, H. Zhang, H. Zhang, S. Zhang, and Z. Cheng, "Three-dimensional magnetotelluric imaging of the SE Gonghe basin: implication for the orogenic uplift in the northeastern margin of the Tibetan Plateau," *Tectonophysics*, vol. 789, article 228525, 2020.

[31] S. Hang, "TetGen, a Delaunay-based quality tetrahedral mesh generator," *Acm Transactions on Mathematical Software*, vol. 41, no. 2, p. 11, 2015.

[32] E. R. Niblett and C. Sayn-Wittgenstein, "Variation of electrical conductivity with depth by the magneto-telluric method," *Geophysics*, vol. 25, no. 5, pp. 998–1008, 1960.

[33] Z. Ye, R. Gao, Z. Lu et al., "A lithospheric-scale thrust-wedge model for the formation of the northern Tibetan Plateau margin: evidence from high-resolution seismic imaging," *Earth and Planetary Science Letters*, vol. 574, article 117170, 2021.

[34] A. Zuza, X. Cheng, and A. Yin, "Testing models of Tibetan Plateau formation with Cenozoic shortening estimates across the Qilian Shan–Nan Shan thrust belt," *Geosphere*, vol. 12, no. 2, pp. 501–532, 2016.

[35] T. Ye, X. Chen, Q. Huang, L. Zhao, Y. Zhang, and M. Uyeshima, "Bifurcated crustal channel flow and seismogenic structures of intraplate earthquakes in Western Yunnan, China as revealed by three-dimensional magnetotelluric imaging," *Journal of Geophysical Research: Solid Earth*, vol. 125, no. 9, 2020.

[36] L. Zhang, M. Unsworth, S. Jin et al., "Structure of the Central Altyn Tagh fault revealed by magnetotelluric data: new insights into the structure of the northern margin of the India-Asia collision," *Earth and Planetary Science Letters*, vol. 415, pp. 67–79, 2015.

[37] X. Gao, B. Guo, J. Chen, Q. Liu, S. Li, and Y. Li, "Rebuilding of the lithosphere beneath the western margin of Ordos: evidence from multiscale seismic tomography," *Chinese Journal of Geophysics*, vol. 61, no. 7, pp. 2736–2749, 2018.

[38] Z. Ye, Q. Li, R. Gao et al., "Anisotropic regime across northeastern Tibet and its geodynamic implications," *Tectonophysics*, vol. 671, pp. 1–8, 2016.

[39] X. Huang, R. Gao, W. Li, and X. Xiong, "Seismic reflection evidence of crustal duplexing and lithospheric underthrusting beneath the western Qilian Mountains, northeastern margin of the Tibetan Plateau," *Science China Earth Sciences*, vol. 64, no. 1, pp. 96–109, 2021.

[40] B. Meyer, P. Tapponnier, L. Bourjot et al., "Crustal thickening in Gansu-Qinghai, lithospheric mantle subduction, and oblique, strike-slip controlled growth of the Tibet Plateau," *Geophysical Journal International*, vol. 135, no. 1, pp. 1–47, 1998.

[41] W. Wang, E. Kirby, Z. Peizhen et al., "Tertiary basin evolution along the northeastern margin of the Tibetan Plateau: evidence for basin formation during Oligocene transtension," *Bulletin*, vol. 125, no. 3-4, pp. 377–400, 2013.

[42] Z. Zhang, Z. Bai, S. Klemperer et al., "Crustal structure across northeastern Tibet from wide-angle seismic profiling: constraints on the Caledonian Qilian orogeny and its reactivation," *Tectonophysics*, vol. 606, pp. 140–159, 2013.

[43] S. Jin, W. Wei, S. Wang, G. F. Ye, M. Deng, and H. D. Tan, "Discussion of the formation and dynamic signification of the high conductive layer in Tibetan crust," *Chinese Journal of Geophysics*, vol. 53, no. 10, pp. 2376–2385, 2010.

[44] M. Unsworth, A. Jones, W. Wei et al., "Crustal rheology of the Himalaya and southern Tibet inferred from magnetotelluric data," *Nature*, vol. 438, no. 7064, pp. 78–81, 2005.

[45] T. Yoshino and F. Noritake, "Unstable graphite films on grain boundaries in crustal rocks," *Earth and Planetary Science Letters*, vol. 306, no. 3-4, pp. 186–192, 2011.

[46] Q. Li, Y. Zhang, Y. Tu, and B. Fan, "The combined interpretation of crustal velocity and electrical resistivity in Qilian Shan mountain-Hexi Corridor region," *Chinese Journal of Geophysics*, vol. 2, pp. 197–210, 1998.

[47] M. Unsworth, W. Wei, A. G. Jones et al., "Crustal and upper mantle structure of northern Tibet imaged with magnetotelluric data," *Journal of Geophysical Research: Solid Earth*, vol. 109, no. B2, 2004.

[48] W. Wei, M. Unsworth, A. Jones et al., "Detection of widespread fluids in the Tibetan crust by magnetotelluric studies," *Science*, vol. 292, no. 5517, pp. 716–719, 2001.

[49] C. Xie, S. Jin, W. Wei et al., "Crustal electrical structures and deep processes of the eastern Lhasa terrane in the south Tibetan Plateau as revealed by magnetotelluric data," *Tectonophysics*, vol. 675, pp. 168–180, 2016.

[50] D. Worrall, V. Kruglyak, F. Kunst, and V. Kuznetsov, "Tertiary tectonics of the Sea of Okhotsk, Russia: far-field effects of the India-Eurasia collision," *Tectonics*, vol. 15, no. 4, pp. 813–826, 1996.

[51] Y. Wang, X. Chen, Y. Zhang et al., "Superposition of cretaceous and Cenozoic deformation in northern Tibet: a far-field response to the tectonic evolution of the Tethyan orogenic system," *GSA Bulletin*, vol. 134, no. 1-2, pp. 501–525, 2022.

[52] K. R. Wilks and N. L. Carter, "Rheology of some continental lower crustal rocks," *Tectonophysics*, vol. 182, no. 1-2, pp. 57–77, 1990.

[53] P. Zhao, J. Chen, Q. Liu, Y. Chen, and Y. Li, "Growth of northern Tibet: insights from the crustal shear wave velocity structure of the Qilian Shan orogenic belt," *Geochemistry, Geophysics, Geosystems*, vol. 22, no. 9, 2021.

[54] Q. Xiao, J. Zhang, G. Zhao, and J. Wang, "Electrical resistivity structures northeast of the eastern Kunlun fault in the northeastern Tibet: tectonic implications," *Tectonophysics*, vol. 601, pp. 125–138, 2013.

[55] S. Xue, Y. Chen, H. Liang et al., "Deep electrical resistivity structure across the Gyaring Co fault in Central Tibet revealed by magnetotelluric data and its implication," *Tectonophysics*, vol. 809, article 228835, 2021.

[56] P. Wannamaker, "Electrical conductivity of water-undersaturated crustal melting," *Journal of Geophysical Research: Solid Earth*, vol. 91, no. B6, pp. 6321–6327, 1986.

[57] F. Le Pape, A. Jones, M. Unsworth et al., "Constraints on the evolution of crustal flow beneathNorthernTibet," *Geochemistry, Geophysics, Geosystems*, vol. 16, no. 12, pp. 4237–4260, 2015.

[58] C. Rosenberg and M. Handy, "Experimental deformation of partially melted granite revisited: implications for the continental crust," *Journal of Metamorphic Geology*, vol. 23, no. 1, pp. 19–28, 2005.

[59] X. Bao, X. Song, M. Xu et al., "Crust and upper mantle structure of the North China Craton and the NE Tibetan Plateau and its tectonic implications," *Earth and Planetary Science Letters*, vol. 369-370, pp. 129–137, 2013.

[60] Q. Wang, Y. Gao, Y. Shi, and J. Wu, "Seismic anisotropy in the uppermost mantle beneath the northeastern margin of Qinghai-Tibet Plateau: evidence from shear wave splitting of SKS, PKS and SKKS," *Chinese Journal of Geophysics*, vol. 56, no. 3, pp. 892–905, 2013.

[61] H. Zhang, Y. Gao, Y. Shi, X. Liu, and Y. Wang, "Tectonic stress analysis based on the crustal seismic anisotropy in the northeastern margin of Tibetan Plateau," *Chinese Journal of Geophysics*, vol. 55, no. 1, pp. 95–104, 2012.

[62] X. Chen, Z. Shao, X. Xiong et al., "Early Cretaceous overthrusting of Yumu Mountain and hydrocarbon prospect on the northern margin of the Qilian Orogenic Belt," *Acta Geoscientica Sinica*, vol. 40, no. 3, pp. 377–392, 2019.

[63] A. Zuza, C. Wu, R. Reith et al., "Tectonic evolution of the Qilian Shan: an early Paleozoic orogen reactivated in the Cenozoic," *GSA Bulletin*, vol. 130, no. 5-6, pp. 881–925, 2018.

[64] P. Wessel and W. Smith, "New, improved version of generic mapping tools released," *Eos, Transactions American Geophysical Union*, vol. 79, no. 47, pp. 579–579, 1998.